Available online at www.sciencedirect.com
ScienceDirect
Solid-State Electronics 51 (2007) 982–988
SOLID-STATE ELECTRONICS
www.elsevier.com/locate/sse

A study of ion implantation into crystalline germanium

R. Wittmann *, S. Selberherr

Institute for Microelectronics, TU Wien Gußhausstraße 27–29/E360, 1040 Wien, Austria

Received 2 February 2007; received in revised form 23 March 2007; accepted 26 March 2007

The review of this paper was arranged by Prof. A. Zaslavsky

Abstract

We report an experimental and simulation study for introducing dopant ions into (100) germanium in the energy range from 5 to 40 keV. The successful calibration of our Monte Carlo ion implantation simulator for amorphous and crystalline Ge targets is demonstrated by comparison of predicted boron profiles with SIMS data. The implantation profile in Ge is shallower than in Si for a given energy due to the larger nuclear and electronic stopping power of Ge atoms. The generated point defects and amorphized regions in the crystal are calculated by a modified Kinchin–Pease model. We found that the higher displacement energy in Ge, the stronger backscattering effect, and the smaller energy transfer from the ion to the primary recoil of a cascade are mainly responsible for the significantly reduced implantation damage in Ge. The point responses for boron implantations in Si and Ge are compared with each other. Finally the simulation results for the formation of interdigitated Ge-on-Si PIN-photodiodes are presented.
© 2007 Elsevier Ltd. All rights reserved.

Keywords: Monte Carlo implantation in germanium; Implantation-induced point defects; Kinchin–Pease model; Photodetector

1. Introduction

Germanium has regained attention in the semiconductor industry for future silicon-compatible optoelectronic and advanced CMOS devices. The carriers have lower effective masses and the intrinsic mobility is about two times higher for electrons and four times higher for holes in germanium compared to silicon. Therefore, germanium offers the highest performance enhancement potential for channel engineering compared to bulk SiGe or strained silicon. On the one hand side, the smaller band gap of germanium is advantageous to build photodetectors and, on the other hand side, junctions made in a smaller band gap material will typically exhibit larger leakage currents. However, deep-submicron germanium-based MOS transistors have been processed in a silicon-like process flow by using either germanium oxynitride (GeO_xN_y) [1] or hafnium oxide (HfO_2) based high-k dielectrics [2,3] as the gate insulator. It was found in [3] that the junction leakage is about four decades higher for germanium at a chip temperature of 110 °C compared with silicon. The reduction of the relatively large leakage current will be a key issue for Ge-CMOS technology to obtain devices with reasonably low off-current. It was reported in [1], that the leakage current of germanium junctions can be reduced down to the order of 10^{-4} A/cm^2 with annealing at 400 °C, which is considered acceptable for MOS transistors. Germanium has also been recognized as a promising material for photodetectors in fibre-optical transmission systems due to the high- optical absorption coefficient for an operation at a wavelength of 1.3 μm in the near infrared (NIR) regime [4,5]. The use of epitaxial Ge-on-Si technology allows the integration of germanium PIN-photodiodes with CMOS circuits on a silicon chip to build optical communication receivers with low fabrication costs. Optical chip-to-chip communication solutions and even optical on-chip

* Corresponding author. Tel.: +43 1 58801/36040; fax: +43 1 58801/36099.
E-mail address: Wittmann@iue.tuwien.ac.at (R. Wittmann).

0038-1101/$ - see front matter © 2007 Elsevier Ltd. All rights reserved.
doi:10.1016/j.sse.2007.03.019

interconnects will be required to meet the challenges of differentiated, high-performance systems in the future.

Ion implantation is a crucial step for processing these device structures. While ion-implanted dopant profiles are well studied in silicon for various dopant species and implantation conditions, dopant profiles are scarce in SiGe alloys as well as in pure Ge. An accurate and multi-dimensional simulation of ion implantation is required for these high-mobility materials to optimize the doping profiles for advanced devices.

2. Modeling of ion implantation in germanium

Our Monte Carlo ion implantation simulator MCIMPL-II [6] is based on a physical BCA method and uses the universal ZBL potential [7]. Lattice vibrations are considered by the Debye model with a Debye temperature of 450 K. An empirical electronic stopping model is used [8] and the generated point defects are calculated by a modified Kinchin–Pease model [9] together with a point defect recombination model. The simulator can handle complex three-dimensional device structures consisting of various amorphous materials and group-IV-based crystalline materials [10].

Silicon and germanium, which both crystallize in the diamond lattice structure, are completely miscible forming $Si_{1-x}Ge_x$ solids with x ranging from 0 to 1. We extended the target materials of the simulator from crystalline silicon to the class of $Si_{1-x}Ge_x$ alloys and Ge by adjusting the lattice parameter $a(x)$ of the crystalline model as function of the Ge fraction x according to

$$a(x) = 0.002733x^2 + 0.01992x + 0.5431 \text{ (nm)} \quad (1)$$

which approximates experimental data with a maximum deviation of about 10^{-4} nm [11]. While the ion moves through the simulation domain, a local crystal model (as shown in Fig. 1) is built up around the actual ion position for searching the next collision partner. The selection of the target atom species for $Si_{1-x}Ge_x$ alloys is defined by probability x for Ge and $(1-x)$ for Si, respectively. In a screened Coulomb collision the energy loss of the ion, ΔE, is equal to the transferred energy to the recoil atom,

$$\Delta E = \frac{4M_1M_2}{(M_1+M_2)^2} \cdot \sin^2\frac{\Theta}{2} \cdot E_0 \quad (2)$$

where M_1 and M_2 are the masses of ion and target atom, Θ is the transformed scattering angle in the center-of-mass coordinates, and E_0 is the kinetic energy of the ion before the collision event [12]. From this equation it can be derived that a smaller energy loss ΔE occurs in nuclear collisions in Ge targets due to the different masses of ion and atom. The transferred energy ΔE from a boron ion to a Ge atom is approximately the half (0.568-fold) compared to ΔE in Si at a given scattering angle. Note that the difference in masses between boron and germanium leads also to a stronger backscattering effect which produces shallower profiles.

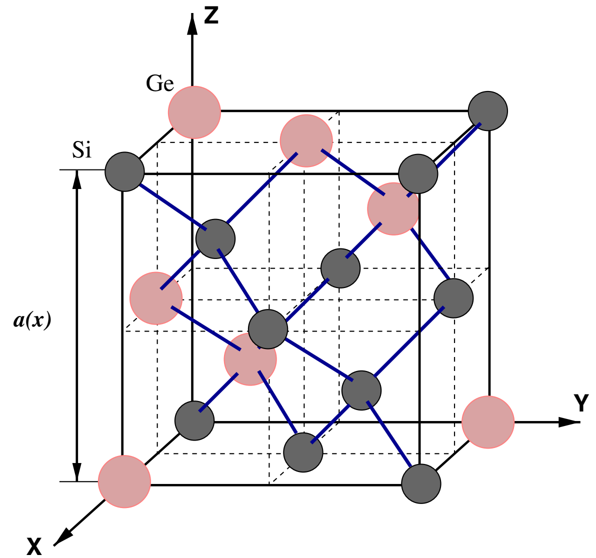

Fig. 1. Local crystal model used for the simulation of ion implantation in Si, $Si_{1-x}Ge_x$ alloys of arbitrary Ge content, and pure Ge ($0 \leqslant x \leqslant 1$).

An advantage of the Monte Carlo simulation is that the used Kinchin–Pease model allows to estimate the produced vacancies in the germanium crystal. Note that equal local concentrations of vacancies and interstitials are assumed, since the recoils themselves are not individually followed in our computationally fast simulation approach. However, a critical model parameter is the threshold displacement energy required for the ion to displace a target atom. A displacement energy E_d of 15 eV has become widely accepted for silicon. We fitted a value of $E_d = 30$ eV for germanium by comparing simulated boron profiles with SIMS measurements. Fig. 2 shows the number of produced point defects for a damage cascade, calculated with the modified Kinchin–Pease model. The value for the displacement energy in germanium is in good agreement with $E_d = 31$ eV which was deduced by Mitchell in 1957 for germanium [13]. The larger E_d value is responsible for

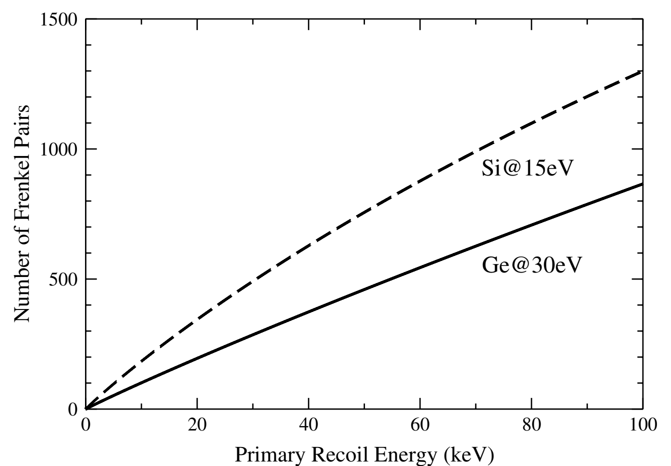

Fig. 2. Number of Frenkel pairs generated by a primary knock-on atom in Si assuming $E_d = 15$ eV and in Ge assuming $E_d = 30$ eV.

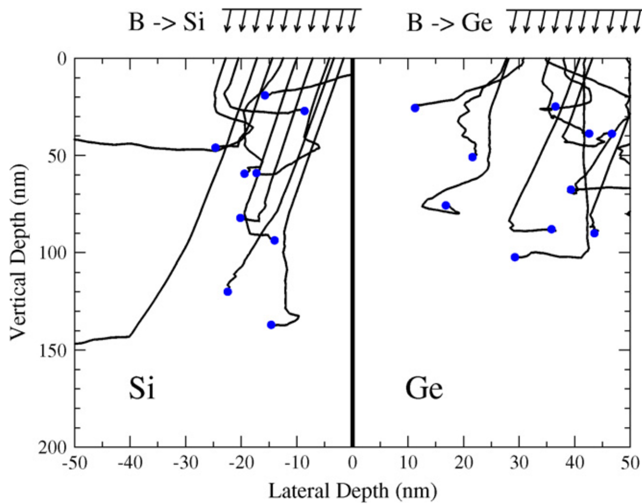

Fig. 3. Comparison of the Monte Carlo simulation of ten boron trajectories in silicon and in germanium using an energy of 10 keV and a tilt of 7°.

the generation of significantly fewer point defects by a boron ion in germanium compared with silicon, which holds true for any amount of transferred energy ΔE to the primary knock-on atom of a cascade. The reduced damage production by ion implantation in crystalline germanium is consistent with former experimental observations [14].

The calibration of the simulator for germanium was performed by adjusting the Lindhard correction parameter k_L of the empirical electronic stopping model. We used the parameter value $k_L = 1.75$ for the boron implantation in silicon and 1.9 for germanium.

The Monte Carlo method is based on computing a large number of individual ion trajectories in the simulation domain with appropriately scaled random numbers. After performing the calculation, the dopant and damage data are both stored in histogram cells aligned on an orthogonal grid. The result is then smoothed and translated from the internal orthogonal grid to an unstructured destination grid suitable for the subsequent simulation of annealing processes. In the following simulation study at least 10^6 trajectories were calculated for a one-dimensional boron profile. Fig. 3 shows the visualization of ten arbitrarily selected boron trajectories in silicon and in germanium. This comparison demonstrates that the larger nuclear and electronic stopping power of germanium, in particular the stronger backscattering of boron ions in germanium, typically reduces the trajectory length.

3. Simulation results and discussion

Germanium has a larger nuclear and electronic stopping power for incoming ions due to the heavier atomic mass and higher electron density. For this reason, an implanted dopant profile in germanium is significantly shallower than in silicon and SiGe for any given implantation energy. Fig. 4 shows that the calibrated simulator can accurately

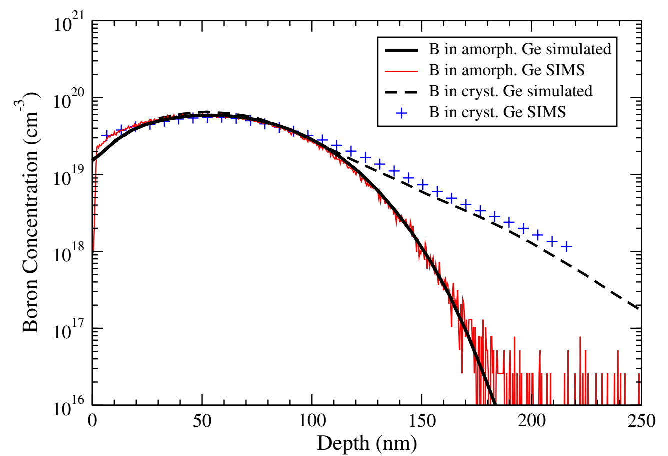

Fig. 4. Simulated 20 keV boron implant profiles in amorphous Ge and in (100) Ge using a dose of 6×10^{14} cm^{-2} and a tilt of 7° compared to SIMS data.

reproduce the measured 20 keV boron concentration profiles implanted with a dose of 6×10^{14} cm^{-2} in amorphous and in crystalline germanium targets. All implantation experiments were performed at room temperature and no twist was used. The amorphization of germanium was performed by the implantation of ^{72}Ge ions with an energy of 200 keV and a dose of 10^{15} cm^{-2}. A channeling tail can be observed for the profile in crystalline germanium. Fig. 5 demonstrates good agreement between the simulated and measured boron profiles implanted with a lower energy of 5 keV and a lower dose of 3×10^{13} cm^{-2}. Fig. 6 compares simulated 20 keV boron profiles in silicon and in germanium. We found the projected range R_p of the boron distribution in $Si_{0.5}Ge_{0.5}$ at a depth of 65 nm, which lies well within the boundaries defined by the projected ranges in germanium at 55 nm and in silicon at 80 nm. Table 1 summarizes simulated and measured R_p and σ_p parameters for boron implants in crystalline silicon, $Si_{0.5}Ge_{0.5}$, and germanium targets. The projected range R_p is read off at the

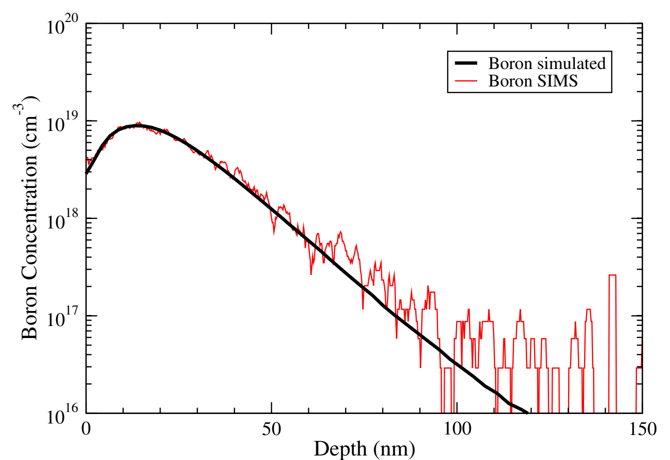

Fig. 5. Simulated 5 keV boron profile in (100) Ge using a dose of 3×10^{13} cm^{-2} and a tilt of 7° compared to SIMS measurement.

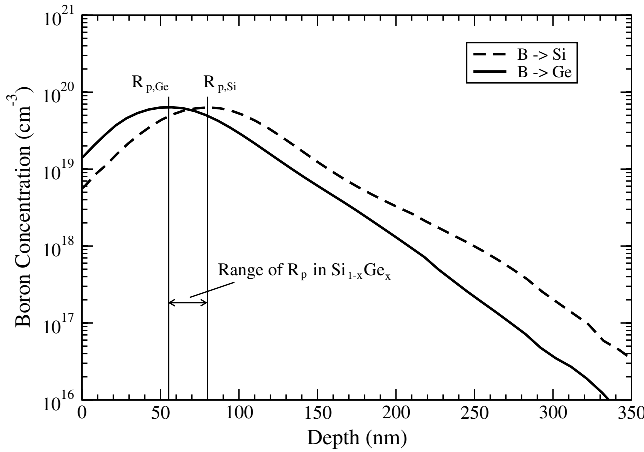

Fig. 6. Comparison of simulated 20 keV boron implant profiles in silicon and germanium using a dose of 6×10^{14} cm^{-2} and a tilt of 7°.

Table 1
Projected range and straggling for boron distributions

Cryst. Material	Si	$Si_{0.5}Ge_{0.5}$	Ge	Si	$Si_{0.5}Ge_{0.5}$	Ge
Energy (keV)	5	5	5	20	20	20
R_p (nm)	18.91	15.44	14.32	79.52	65.32	55.27
σ_p (nm)	14.16	12.56	12.16	37.42	36.33	39.38
SIMS R_p (nm)	–	–	16.23	–	67.11	56.99
SIMS σ_p (nm)	–	–	11.23	–	40.58	34.91

maximum concentration of a boron distribution and the provided straggling σ_p is the average value of the left and right straggling values which are determined by 60% of the maximum boron concentration. The results in the table were obtained with an implantation dose of 10^{14} cm^{-2} and a tilt of 7°.

Fig. 7 compares the simulated vacancy concentration profiles in silicon and in germanium associated with the 20 keV boron implantations shown in Fig. 6. The vacancy maximum is not at the wafer surface, since the electronic stopping process dominates at high-initial ion energies. A boron ion enters most likely a channel at the surface and despite of the tilted incident direction it can stay at least a short distance inside a channel. The higher displacement energy of 30 eV, the stronger backscattering of boron ions in germanium, and the smaller energy transfer ΔE from the ion to the primary recoil of a cascade are mainly responsible for the significantly smaller damage production in germanium. Previous experimental boron implantation results in germanium [14] performed up to a dose of 10^{14} cm^{-2} within the energy range of 25–150 keV revealed that 100% of the boron ions are immediately active after implantation without thermal annealing. This is a unique phenomenon, since an annealing step is required for every other dopant species implanted in silicon or germanium in order to activate a significant amount of dopants. Fig. 8 illustrates the dose dependence of 40 keV boron profiles in germanium simulated with the Kinchin–Pease damage model. It is obvious that the shape of the profiles is influenced by the damage accumulation in the crystal.

The simulated point responses in crystalline silicon and germanium are shown in Figs. 9 and 10, respectively, to study quantitatively the lateral and vertical penetration of boron ions. The used two-and-a-half dimensional geometry has a depth dimension of 40 nm, and the slot width of the implantation window in the impenetrable mask is 8 nm. A high-resolution mesh which consists of 33181 grid points and 144159 tetrahedrons is added to the input structure to resolve the implanted boron distribution. Boron is implanted with an energy of 10 keV, a dose of 5×10^{15} cm^{-2}, and the ion beam is 7° tilted in such a way that the lateral component of the incident direction is parallel to the direction of view ($\langle 010 \rangle$ direction). Therefore, the presented point responses are symmetric. Approximately 420000 simulated boron ions enter the substrate at the mask opening and contribute to the Monte Carlo result represented by histogram cells. The comparison of the point responses indicate that the boron distribution in

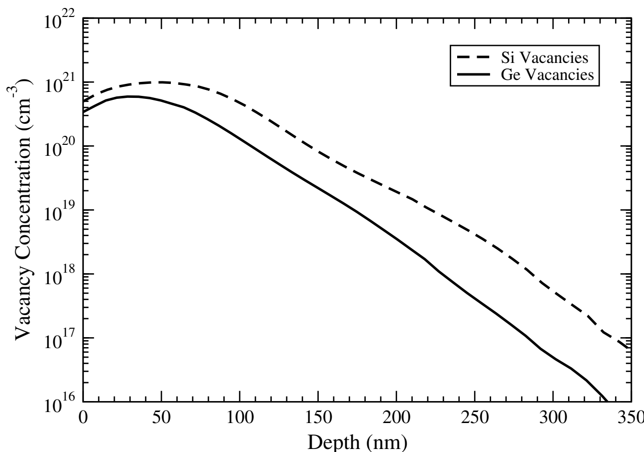

Fig. 7. Comparison of produced vacancies for the 20 keV boron implantations in silicon and germanium using a dose of 6×10^{14} cm^{-2} and a tilt of 7°.

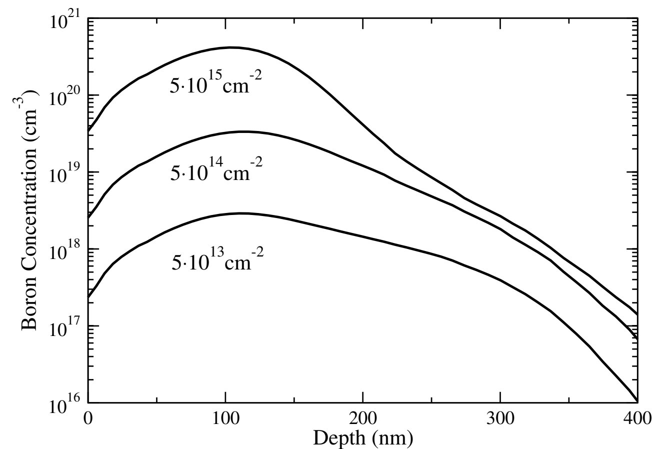

Fig. 8. Simulated 40 keV boron implants in (1 0 0) Ge at doses of 5×10^{13}, 5×10^{14}, and 5×10^{15} cm^{-2} using a tilt of 7°.

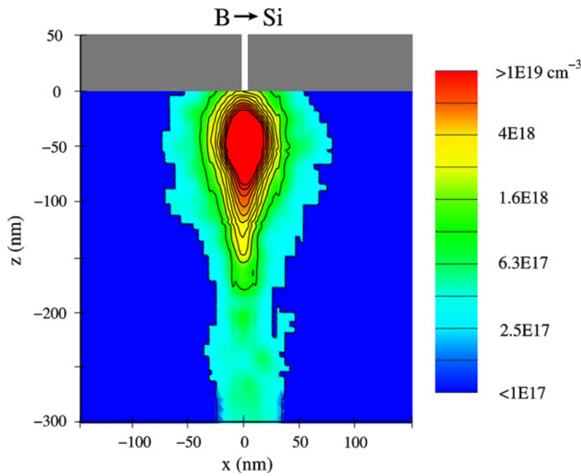

Fig. 9. Simulated point response for a 10 keV high-dose implantation of boron into crystalline silicon.

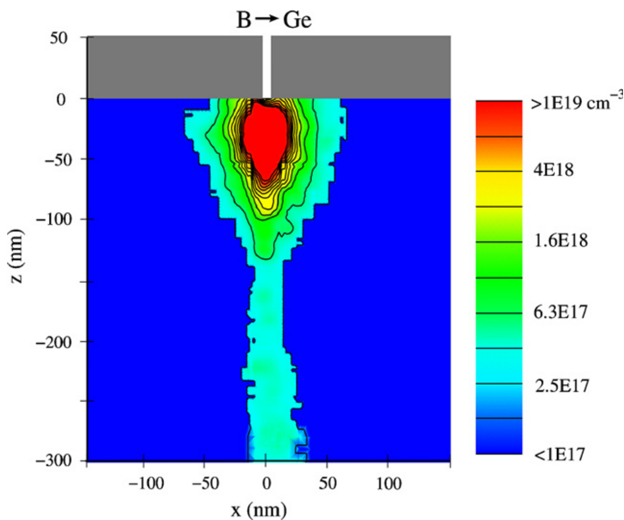

Fig. 10. Simulated point response for a 10 keV high-dose implantation of boron into crystalline germanium.

germanium is significantly reduced in vertical direction, while the lateral profile is quite similar in silicon and germanium. In addition, it can be observed that the channeling tail is closely centered around the $\langle 100 \rangle$ axis in both cases. This demonstrates that in (100) silicon and in (100) germanium, axial channeling in the $\langle 100 \rangle$ direction dominates by far over channeling in other directions.

4. Formation of interdigitated Ge PIN-photodiodes

In optical transmission systems, an operation at 1.3 μm and 1.55 μm wavelengths is preferred due to the low attenuation in fiber-optic cables. Germanium is an attractive candidate for high-speed photodetector applications due to its high-electron mobility and high-optical absorption coefficient in this wavelength range [15]. Recently, a bandwidth of 10 GHz has been demonstrated at a wavelength of 1.3 μm for a PIN-photodiode, fabricated in epitaxial Ge-on-Si technology [5]. The use of germanium is advantageous over III–V compound materials in terms of lower fabrication costs and feasible integration with silicon CMOS technology. Therefore, the calibrated ion implantation simulator was applied to study the dopant and damage distributions in a germanium PIN-photodiode in order to facilitate the processing of such devices.

Compositionally graded SiGe layers are deposited on the silicon wafer to achieve a 1 μm thick germanium layer with a low defect density. In this doping application, the interdigitated p^+ – and n^+-finger regions of the photodetector are formed by ion implantation. For this purpose, photoresist masks are used to define the finger structure with a width of 1 μm and a spacing of 2 μm. Fig. 11 shows the schematic top and cross-sectional views of the final PIN-photodetector. This large area photodetector consists of elementary photodiodes which are connected in parallel. An elementary photodiode can be defined as the three-dimensional region from the center of a p^+-finger to the center of an n^+-finger. In the first process step the p^+-fingers are patterned and boron is implanted with an energy of 15 keV and a dose of 2×10^{15} cm^{-2}. The three-dimensional boron distribution, as shown in Fig. 12, was

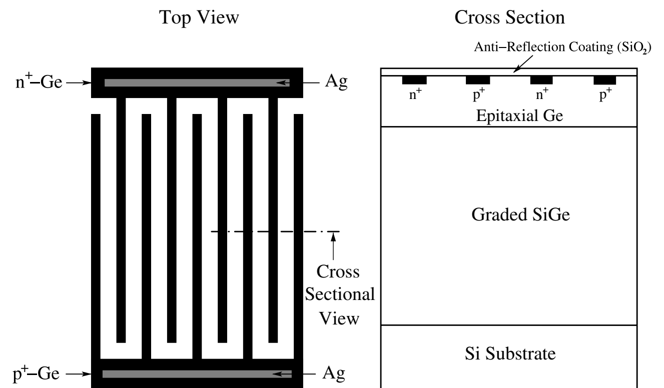

Fig. 11. Layout (left) and cross-section (right) of a high-speed Ge-on-Si PIN photodetector with planar interdigitated p^+- and n^+-fingers.

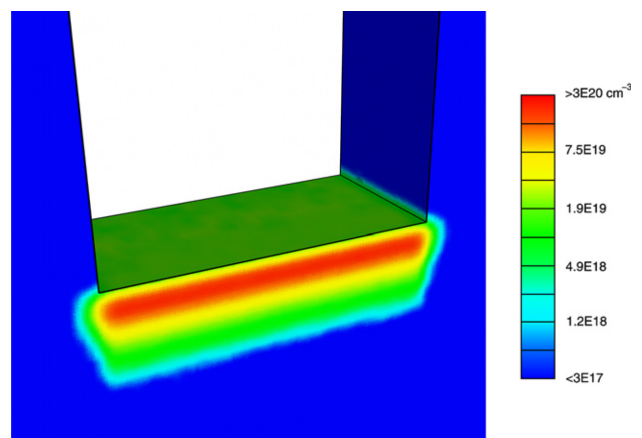

Fig. 12. Simulated 15 keV boron implantation step for the p^+-finger formation in germanium using a photoresist mask.

obtained by using a 5 nm thick oxide scattering layer on top of germanium. In the second process step the n^+-fingers are formed by an implantation of arsenic with an energy of 60 keV and same dose. The shallow arsenic distribution in the simulated device part is presented in Fig. 13. In spite of the lower implantation energy, boron ions can penetrate much deeper into the germanium layer than arsenic ions. Fig. 14 allows to compare the simulated boron and arsenic profiles in the PIN-photodiode by using equal doping concentration isolines. The reason for the large channeling tail of the boron profile lies mainly in the small amount of produced point defects in germanium. The critical level of point defects (Frenkel pairs) needed for amorphization of germanium is about 4.42×10^{21} cm^{-3}, one tenth of the germanium atomic density [16]. Fig. 15 demonstrates that the arsenic implantation has produced an amorphous zone, while the maximum defect concentration of the boron implantation is significantly lower than the amorphization level. The predicted damage results are consistent with experimental observations obtained by processing a PIN-photodiode on a germanium substrate under similar process conditions. In [17] it was found that the as-implanted resistance of the boron implant was 201 Ω/□ at a dose of 2×10^{15} cm^{-2}, while that for the arsenic implant was not measurable. This fact strongly indicates that boron-implanted germanium remains crystalline at least up to the used dose, while arsenic-implanted germanium becomes amorphous.

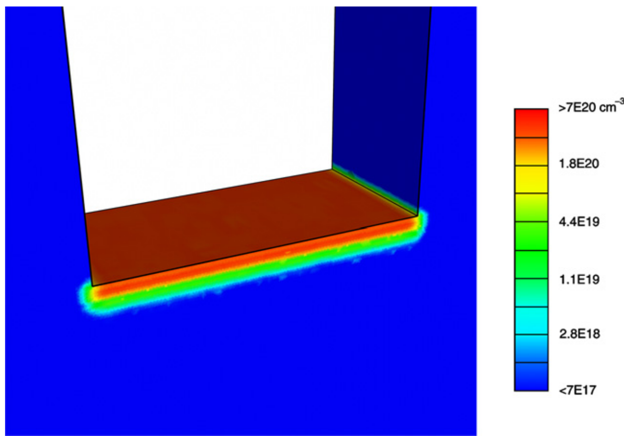

Fig. 13. Simulated 60 keV arsenic implantation step for the n^+-finger formation in germanium using a photoresist mask.

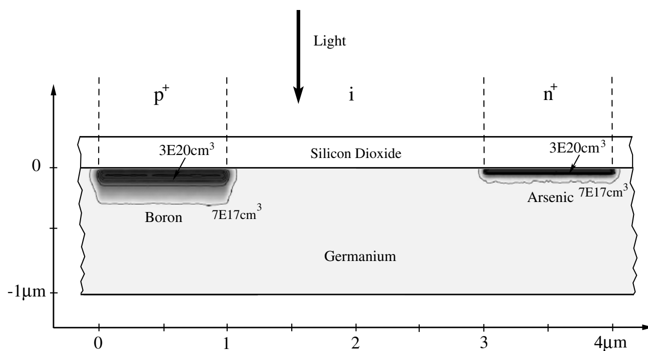

Fig. 14. Simulated doping concentration isolines in the p^+- and n^+-fingers of an elementary PIN-photodiode of the detector in the cross-sectional view.

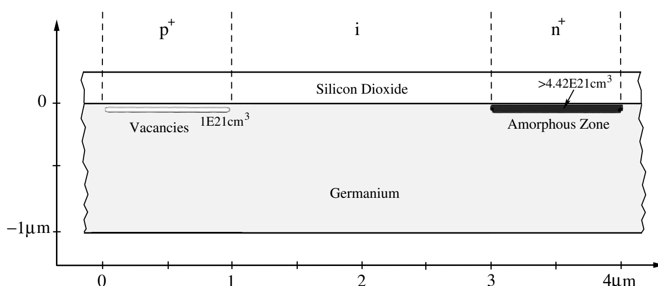

Fig. 15. Simulated amorphization of germanium in the finger regions after the boron and arsenic implantations with a dose of 2×10^{15} cm^{-2}.

5. Summary and conclusions

Dopant implantation, generation of point defects, and channeling have been investigated in germanium by using a physics-based simulation approach and experimental data. We showed that our calibrated Monte Carlo ion implantation simulator can accurately predict the dopant profiles in amorphous and crystalline germanium materials. We found that the implantation-induced vacancy concentration in germanium is significantly reduced compared to silicon, which is consistent with former experimental studies indicating that boron-implanted germanium remains essentially crystalline. The simulated point responses revealed that the dopant distribution is significantly reduced in vertical direction, while the lateral profile is quite similar in silicon and germanium. Finally, the boron and arsenic implantation results for processing of interdigitated PIN-photodiodes in a Ge-on-Si substrate are discussed.

Acknowledgements

We are indebted to Dr. Suresh Uppal from the University of Newcastle upon Tyne for providing SIMS data and background information about the experiments.

References

[1] Shang H, Okorn-Schmidt H, Chan KK, Copel M, Ott JA, Kozlowski PM, et al. High-mobility p-channel germanium MOSFETs with a thin Ge oxynitride gate dielectric. In: Proceedings of the intternational electron devices meeting (IEDM); 2002. p. 441–4.

[2] Delabie A, Puurunen RL, Brijs B, Caymax M, Conard T, Onsia B, et al. Atomic layer deposition of hafnium oxide on germanium substrates. J Appl Phys 2005;97(6):1–10.

[3] Meuris M, De Jaeger B, Kubicek S, Verheyen P, Van Steenbergen J, Lujan G, et al. Germanium deep-submicron PMOS transistors with etched TaN metal gate on a high-k dielectric, fabricated in a 200 mm

prototyping line. In: ECS, editor. Proceedings of the SiGe: materials, processing, and devices, vol. 2004–2007. Honolulu, USA: Electrochemical Society; 2004. p. 693–700.

[4] Jones RE, Thomas SG, Bharatan S, Thoma R, Jasper C, Zirkle T, et al. Fabrication and modeling of gigahertz photodetectors in heteroepitaxial Ge-on-Si using a graded buffer layer deposition by low energy plasma enhanced CVD. In: Proceedings of the international electron devices meeting (IEDM); 2002. p. 793–6.

[5] Colace L, Balbi M, Masini G, Assanto G, Luan HC, Kimerling LC. Ge on Si PIN-photodiodes operating at 10 Gb/s. J Appl Phys 2006;88(10):1–3.

[6] Wittmann R, Hössinger A, Selberherr S. Improvement of the statistical accuracy for the three-dimensional Monte Carlo simulation of ion implantation. In: Proceedings of the 15th European simulation symposium (ESS); 2003. p. 35–40.

[7] Ziegler JF, Biersack JP, Littmark U. The stopping and range of ions in solids. Pergamon Press; 1995.

[8] Hobler G, Simionescu A, Palmetshofer L, Jahnel F, Criegern R, Tian C, et al. Boron channeling implantations in silicon: modeling of electronic stopping and damage accumulation. J Appl Phys 1995;77(8):3697–703.

[9] Norgett MJ, Robinson MT, Torrens IM. A proposed method of calculating displacement dose rates. Nucl Eng Des 1975;33:50–4.

[10] Wittmann R, Hössinger S, Cervenka A, Selberherr J. A study of boron implantation into high Ge content SiGe alloys. In: ECS Transactions, editor. Proceedings of the SiGe: materials, processing, and devices, vol. 3. Cancun, Mexico: Electrochemical Society; 2006. p. 667–76.

[11] Kasper E, Lyutovich K. Properties of silicon germanium and SiGe: carbon. London: Inspec; 2000.

[12] Ziegler JF. Ion implantation – science and technology. Ion Implantation Technology Co.; 1996.

[13] Mitchell EWJ. The effect of radiation damage on the electronic properties of solids. Br J Appl Phys 1957;8:179–89.

[14] Jones KS, Haller EE. Ion implantation of boron in germanium. J Appl Phys 1987;61(7):2469–77.

[15] Oh J. Planar Ge photodetectors on Si substrates for Si/Ge-based optical receivers. Dissertation. University of Texas at Austin, 2004.

[16] Stiebel D, Burenkov A, Pichler P, Cristiano F, Claverie A, Ryssel H. Modeling the amorphization of Si due to the implantation of As, Ge, and Si. In: Proceedings of the international conference on ion implantation technology; 2000. p. 251–4.

[17] Oh J, Csutak S, Campbell JC. High-speed interdigitated Ge PIN photodetectors. IEEE Photon Technol Lett 2002;14(3):369–71.